

Design of Self-Energizing Clutch Actuator for Dual-Clutch Transmission

Jiwon J. Oh, Jinsung Kim, and Seibum B. Choi

Abstract—A novel dry clutch actuator for the dual-clutch transmission (DCT) using self-energizing principle is suggested. A mathematical model of the actuator and the inclusive DCT driveline is developed. The magnitude of torque amplification obtained by the self-energizing effect is studied, and it is verified via experiments by comparing the calculated and the empirical gains. Also, by analyzing the characteristics of the energy consumption in actuator motors during the vehicle launch and gear shifts, the application potential for the self-energizing clutch actuator is examined. Such work is done both through simulation and dynamometer experiments. The simulation is conducted by using the driveline and self-energizing actuator model developed by using MATLAB/Simulink. The hardware-in-the-loop experiments are conducted with the driveline dynamometer that is designed and constructed exclusively for the self-energizing clutch actuator and DCT to experimentally demonstrate the suitability of the suggested actuator for DCT.

Index Terms—Actuation efficiency, clutch actuator, driveline, dual-clutch transmission (DCT), dynamic model, self-energizing effect.

NOMENCLATURE

Actuator Model

θ_m	Actuator motor angle.
θ_a	Actuation plate angle.
F_p	Pinion gear force.
F_n	Clutch engagement force.
μ	Clutch friction coefficient.
N_{ae}	Effective gear ratio.
T_m	Actuator motor torque.
T_a	Actuation plate torque.
T_c	Clutch torque.
α	Rack gear angle.
r_p	Rack gear radius.
R_c	Effective clutch radius.

Manuscript received February 7, 2015; revised May 22, 2015 and August 3, 2015; accepted August 24, 2015. Date of publication September 15, 2015; date of current version February 24, 2016. Recommended by Technical Editor G. Herrmann. This work was supported by the National Research Foundation (NRF) of Korea grant funded by the Korea government (MEST) (2012-0000991) and the Ministry of Science, ICT, and Future Planning (MSIP), Korea, under the Convergence Information Technology Research Center (CITRC) support program (NIPA-2014-H0401-14-1001) supervised by the National IT Industry Promotion Agency (NIPA).

J. J. Oh and S. B. Choi are with the Korea Advanced Institute of Science and Technology (KAIST), Daejeon 34141, Korea (e-mail: jwo@kaist.ac.kr; sbchoi@kaist.ac.kr).

J. Kim is with Hyundai Motor Company, Hwasung 18280, Korea (e-mail: jinsung.kim@hyundai.com).

Color versions of one or more of the figures in this paper are available online at <http://ieeexplore.ieee.org>.

Digital Object Identifier 10.1109/TMECH.2015.2474855

Driveline Model

Variables

ω	Angular speed.
T	Torque.
F	Force.
J	Inertia.
α_{th}	Throttle angle.
θ	Angle
k	Torsional stiffness.
b	Torsional damping coefficient.
i_t	Transmission gear ratio.
i_f	Final reduction gear ratio.

Subscripts

e	Engine.
d	Damper.
c	Clutch.
a	Pressure plate.
t	Transfer shaft.
o	Output.
w	Wheel.
v	Vehicle.
m	Actuator motor.
1	First clutch.
2	Second clutch.

I. INTRODUCTION

UNDENIABLY, increasing the fuel efficiency of ground vehicles has become one of the core technologies among most of the global car manufacturers. Here, the power transmission efficiency in the vehicle powertrain is one of the most significant factors that influence the vehicle's fuel efficiency. Hence, attempts to increase the efficiency of the conventional planetary gear-type automatic transmission (AT) with torque converter have been made through various methods. These include conventional AT with increased number of gears and lock-up clutch [1], continuously variable transmission (CVT) that has replaced the conventional gears with the ones that have continuously variable gear ratio [2]–[4], automated manual transmission (AMT) in which the driver's maneuvers required in manual transmissions are automated through the use of actuators [5], [6], alteration of the synchronizer to resolve the torque intervention issues in AMTs [7], and hybridization of powertrain [8]–[10]. And recently, dual-clutch transmission (DCT) is gaining popularity in the market for its high efficiency in transmitting the power from the engine to the wheels and capability to conveniently, swiftly, and seamlessly perform gearshifts [11], [12].

Although DCTs seem to have all the advantages, further enhancement is required in the actuator mechanism. First of all, DCTs with wet clutch and hydraulic actuators [13]–[15] involve hydraulic pumping and viscous friction loss like ATs that are hydraulically actuated [16], and the efficiency of such system is generally known to be slightly lower than that of the DCTs with dry clutch. The DCTs with dry clutch, mostly actuated electromechanically [17], [18], do have higher efficiency than that of the previously mentioned hydraulically actuated system. However, in order to provide sufficient engagement force in the clutch, the system requires an electromechanical actuator with high power. Since the actuators in the small to mid-size sedans mounted with DCT have the rated output usually between 150 and 300 W for a single clutch, a high amount of electric energy is consumed, which adversely affects the overall fuel efficiency. Moreover, two of such actuators are required, since each clutch in the DCT must be controlled separately.

DCTs lead seamless output torque during a shift by disengaging the off-going clutch simultaneously as engaging the on-coming clutch. In such process, the rate of engagement force variation must be controlled accurately by using the two actuators; otherwise, the powertrain experiences either discontinuous torque, or clutch tie-up via backward torque circulation. To prevent such issues, dry clutch system involves diaphragm spring and flat spring to span the resulting clutch engagement force variation over an elongated range of actuator displacement [19]. This way, by using the predetermined relationship between the engagement force and actuator position [20] in case of the position-controller clutch actuator system, obtaining the desired engagement force with sufficiently high accuracy based on the actuator displacement information is possible. In doing so, however, the amount of energy consumed by the actuator is increased due to elongated actuation distance; hence, it adversely affects the overall fuel efficiency of the vehicle. The weight increase due to the use of diaphragm springs and high-output motors also counts toward the fuel efficiency degradation.

Therefore, this study suggests a self-energizing actuator for the DCTs in replacement of the high-power motor and diaphragm springs. Since the self-energizing mechanism facilitates the motor actuation during clutch engagement by using the energy gained from the frictional loss dissipated in the clutch, power requirement of the actuator can be substantially relieved. In addition, because the mechanism of the self-energizing actuator provides the energizing effect in the on-coming clutch and de-energizing effect in the off-going clutch, the level of control accuracy required for seamless gearshift is reduced. This indicates that the diaphragm spring can be eliminated, which implies further reduction in the amount of energy consumed by the actuators both by weight reduction and actuation stroke reduction.

The ball–ramp mechanism is structurally simple and it surely provides the self-energizing effect. It is in fact widely used to control the torque transmission between axles. However, it is unsuitable for the clutch control where gear shifts are involved, since only the ON/OFF control is possible with the ball–ramp mechanism [21]–[23], and the slip at the contact point of the ball and ramp leads to inconsistency in the relationship between the actuator displacement and engagement force.

A self-energizing actuator using worm shaft mechanism had been developed in the previous effort [24], [25]. This study has validated the engagement force amplification effect, but the mechanism involved high actuator friction during operation due to the use of worm shaft and, most critically, has not examined the application case on DCT.

This paper suggests the self-energizing clutch actuator designed for DCT [26] and examines the effect of self-energizing phenomenon on actuation efficiency during the launch and gear shift process via simulation using the driveline model based on DCT and also the real test bench constructed for this purpose. The organization of the paper is as follows. Section II first describes the hardware and provides details on the operation principle of the self-energizing clutch actuator. Section III deals with the dynamic models of the actuator and driveline so that simulation can be conducted based on the constructed model. In Section IV, simulation results are given and the actuator energy consumption is analyzed under specified scenario. Such work is further verified in Section V by using the actual test bench, which consists of the vehicle driveline dynamometer that includes DCT and the self-energizing clutch actuator.

II. HARDWARE DESCRIPTION FOR SELF-ENERGIZING CLUTCH ACTUATOR AND TEST BENCH

A. Advantage of Self-Energizing Clutch Actuator

The ability of the self-energizing clutch actuator is to cause the driving torque to facilitate the clutch engagement. To realize such mechanism, the pressure plate is designed to approach the clutch disk in a helical shape rather than linearly move and press onto the clutch disk in the direction orthogonal to the friction facing.

The advantages of the suggested actuator for DCT can be listed as follows:

- 1) Energy consumption in actuator motor can be significantly reduced, which leads to further potential for fuel efficiency improvement by adopting DCT.
- 2) Actuator motors with less power output would still suffice for the same torque transmissibility capacity, since the clutch-transferred torque facilitates the actuation torque during engagement. This implies reduced weight and cost for manufacturing.
- 3) Clutch tie-up in DCT can be prevented in case of an actuator failure. During a gear shift, self-energizing effect takes place in the oncoming clutch with positive torque transferred and de-energizing effect takes place in the off-going clutch with negative torque transferred. So severe backward torque circulation, often critical to clutch durability, caused by simultaneous engagement of both clutches can be avoided.
- 4) Elimination of the diaphragm springs in conventional dry DCT leads to further actuation efficiency improvement, since reduction in pressure plate displacement leads to less consumption of irretrievable energy.
- 5) The ad hoc features in the conventional DCT actuators to assist the actuator motor torque by the use of additional

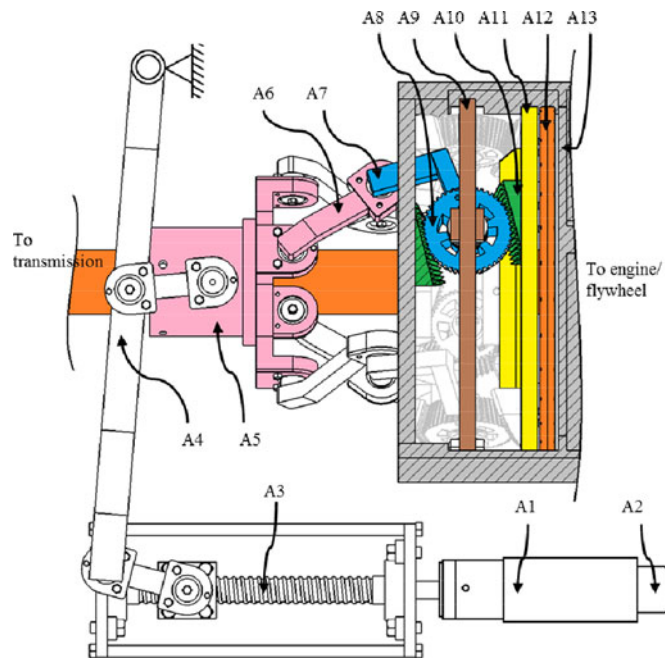


Fig. 1. Self-energizing clutch actuator.

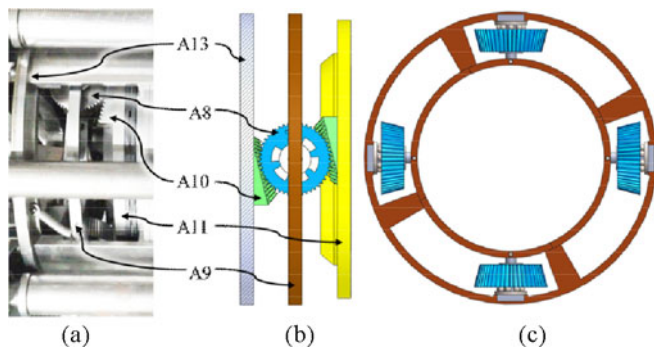


Fig. 2. Pinion gear and inclined rack gears. (a) Constructed system. (b) Top view of the pinion and rack gears. (c) Side view of the pinion gears with retainer.

cams or coil springs are unnecessary, since the driving torque itself facilitates the clutch engagement.

The most distinctive drawback that can be found in the suggested actuator design is the increased system sensitivity. Due to steeper rate of engagement force variation within the actuator motor displacement range, the effect of the varying clutch kissing point on the clutch engagement strength control accuracy in the proposed system is greater than in the conventional system. However, effective software approaches can be taken to deal with such issue, and these may include the use of kissing point compensation [27], [28] and torque observer [11].

B. Self-Energizing Clutch Actuator Hardware

The main components of the self-energizing clutch actuator are indicated in Fig. 1, and the key features of the self-energizing clutch actuator—a pair of inclined rack gears and a pinion gear between them to produce helical motion—are shown in Fig. 2.

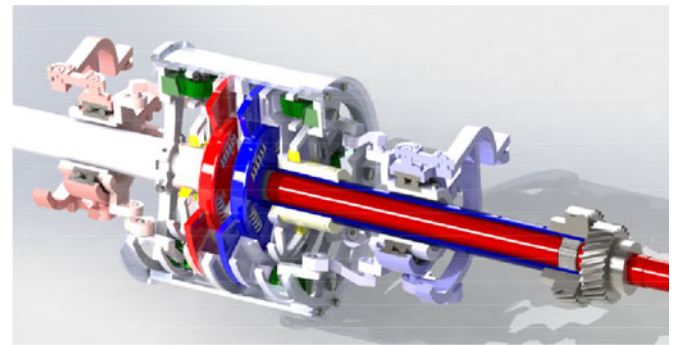


Fig. 3. Two sets of self-energizing clutch actuators and clutches coaxially placed in the actuator housing.

For the engagement of the clutch, the motor (A1) pulls the lever (A4) by applying torque on the ball screw (A3). This causes the lever (A4) to push the thruster (A5) toward the clutch. There are thrust bearings between the lever and the thruster, so that the lever stays stationary while the thruster rotates with the engine. Now, the thrust force at the thruster is transmitted through the upper push rod (A6) and turns the pinion gears (A8). Here, four pinion gears are packaged in the actuator housing along the circumference to maintain force balance, and they are bound in position by the pinion retainer (A9). Each pinion gear is connected to the thruster via separate upper push rods, and each rotates by the equal amount of angle.

The angular displacement of the pinion gear (A8) directly leads to the rotation of the pressure plate (A11). Here, due to the inclined angle of the rack gear (A10), the pressure plate goes through linear displacement toward the clutch disk (A12) as well as angular rotation relative of the actuator housing (A13). When the pressure plate (A11) proceeds toward the clutch disk (A12) and touches the friction facing, the actuator is at its kissing point and torque is transmitted to the clutch disk (A12). When the motor rotates further in the engaging direction, the leaf spring in the clutch disk (A12) is compressed and higher amount of normal force acts between the pressure plate (A11) and clutch disk (A12).

The actuator system depicted in Fig. 1 just shows a single actuator. It must be noted that another actuator is attached symmetrically to control the engagement of the second clutch, and such hardware is shown in Fig. 3. The cut-away view of the dual clutch actuator in Fig. 3 shows two clutch disks and two coaxially positioned input shafts. One clutch is interlocked to the solid input shaft's splines, and another to the hollow input shaft's splines.

C. Driveline Test Bench

The main components of the driveline built to conduct experiments are shown in Fig. 4. The ac motor (D1) plays the role of the vehicle power source, usually an internal combustion engine. To identify the speeds and torques given by the power source, an encoder (D2) and a torque sensor (D3) are attached directly on the shaft connected to the ac motor. In order to damp the possible torque ripple or jerk caused by the ac motor, an external damper (D4) is attached between the motor and the

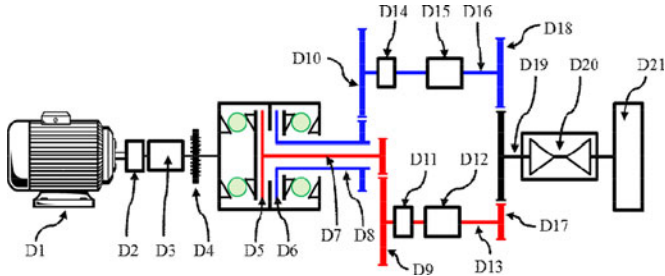


Fig. 4. Formation of the driveline test bench.

clutch actuator housing. The torque is not transmitted to the transmission gear sets unless the actuators apply engagement pressure on the clutches. Clutch 1 (D5) and Clutch 2 (D6) are designed to transmit torque to the input shaft 1 (D7) and input shaft 2 (D8), respectively. In real DCT, input shaft 1 and input shaft 2 would transmit torque to the odd gears and even gears, respectively. The constructed test bench, however, only consists of the first (D9) and second gear (D10) so that launch and gear shifts can be tested. These gears are connected to the transfer shafts (D13 and D16), and each transfer shaft has an encoder installed for the provision of shaft speed information and a torque sensor attached for the validation purpose. Both transfer shafts are designed to transmit torque to a single output shaft (D19) through final reduction gears (D17 and D18). For the wheel speed measurement, an additional encoder is attached on the output shaft. In order to provide the rotational inertia that is equivalent in magnitude to the inertia of a midsize sedan, a planetary reduction gear (D20) is installed in the reverse direction between the output shaft (D19) and the inertia disk (D21) with the calculated dimension.

III. DYNAMIC MODEL

A. Self-Energizing Clutch Actuator Model

In order to validate the increase in actuation efficiency via simulation, dynamic models of the self-energizing actuator and the driveline must be established. Fig. 5 shows the illustration of the actuator model.

The effective gear ratio between the actuator motor and the pressure plate is denoted by N_{ae} , and the angle of rack gear's inclination is denoted by α . Also, r_p , R_c , F_n , F_p , and μ indicate the pinion gear position from the center, the effective clutch radius, the clutch normal force, the pinion gear reaction force, and the clutch friction coefficient, respectively.

Setting up the torque balance equation for the pressure plate gives the following equation:

$$J_a \ddot{\theta}_a = \begin{cases} T_a - T_f, & \text{when disengaged} \\ T_a + T_c - 2r_p F_p \sin \alpha - T_f, & \text{when in contact} \end{cases} \quad (1)$$

Here, T_f is the sum of the friction torque in the actuation route which acts on the pressure plate.

Also, the normal reaction force on the pinion gear can be expressed in terms of the clutch engagement force as shown

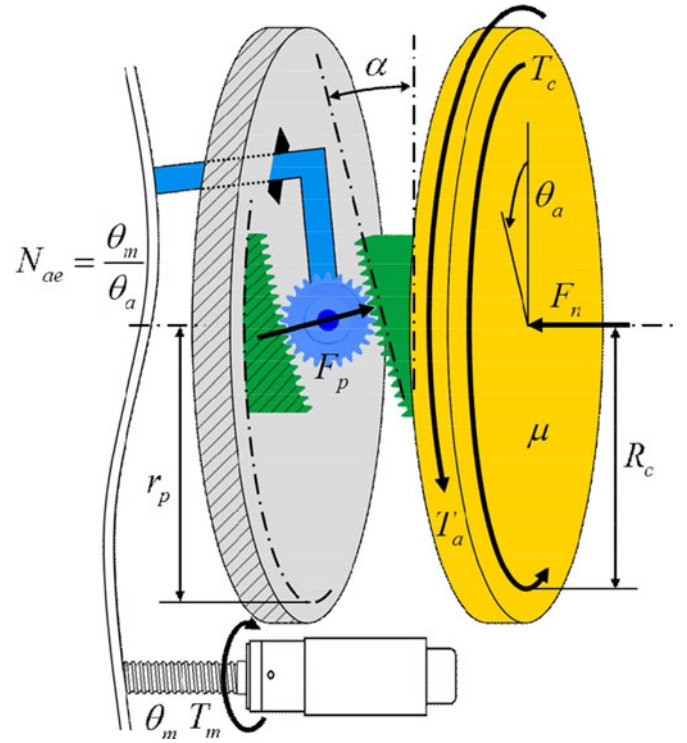


Fig. 5. Self-energizing clutch actuator model.

next

$$F_p = \frac{F_n}{\cos \alpha} \quad (2)$$

Using the aforementioned equation, assuming that actuator parts are rigid bodies, (1) can be converted to the governing equation for the actuation motor, as shown next

$$J_a^* \dot{\omega}_m = \begin{cases} T_m - T_f^*, & \text{when disengaged} \\ T_m + \frac{T_c}{N_{ae}} - \frac{2r_p \tan \alpha}{N_{ae}} F_n - T_f^*, & \text{when in contact} \end{cases} \quad (3)$$

where T_f^* indicates the sum of the friction torque in the actuation route, which acts on the motor, and

$$J_a^* = \frac{J_a}{N_{ae}^2} \quad (4)$$

Here, the clutch normal force is provided based on the empirically calibrated table as a function of the actuator motor angular position.

Then the electrical part of the motor is modeled simply as the following:

$$L_m \frac{di_m}{dt} = -k_e \omega_m - R_m i_m + u_m \quad (5)$$

$$T_m = k_t i_m \quad (6)$$

Here, L_m , k_e , k_t , R_m , u_m , and i_m are the motor inductance, the back-emf constant, the torque constant, the armature resistance, the control input, and the motor current, respectively.

The friction acting on the motor is modeled with LuGre friction model [29] as follows:

$$T_f^*(\omega_m, z) = \sigma_0 z + \sigma_1 \dot{z} + \sigma_2 \omega_m \quad (7)$$

where

$$\dot{z} = \omega_m - \frac{|\omega_m|}{g_s(\omega_m)} z$$

and

$$\sigma_0 g_s(\omega_m) = f_{\text{Coulomb}} + (f_{\text{static}} - f_{\text{Coulomb}}) e^{-(\omega_m / \omega_s)^2}.$$

Here, z , g_s , f_{Coulomb} , f_{static} , and ω_s denote the internal friction state, the Stribeck effect function, the Coulomb friction, the static friction, and the Stribeck velocity, respectively. Also, σ_0 , σ_1 , and σ_2 , respectively, represent the bristle stiffness coefficient, the damping coefficient, and the damping coefficient. These parameters are tuned within the physically plausible range so that the modeled dynamics of the motor is similar to the actual motor dynamics. Here, since the modeled friction must describe the friction acting on the entire actuator dynamics, parameters are tuned without isolating the motor from the actuator parts.

Now, since the system of interest uses dry-type clutch disk, the clutch-transferred torque can be simply modeled as the following:

$$T_c = \mu R_c F_n. \quad (8)$$

B. Torque Transmissibility Characteristic

Let us define actuation gain and torque amplification gain for design specification and torque transmissibility identification

$$G_a \equiv \frac{T_c}{T_a} \quad (9)$$

$$G_t \equiv \frac{T_{c,\text{energizing}}}{T_{c,\text{nonenergizing}}} = \frac{F_{n,\text{energizing}}}{F_{n,\text{nonenergizing}}}. \quad (10)$$

The actuation gain G_a is the ratio of clutch torque to actuation torque on the pressure plate. Greater actuation value indicates that less amount of actuation effort is required to achieve the equivalent level of maximum torque. Negative actuation gain implies a self-locking system, in which the clutch is engaged even without any actuation effort. The torque amplification gain G_t is the ratio of the maximum torque transmissibility with self-energizing effect to that without self-energizing effect. This gain is equivalent to the ratio of clutch engagement force with self-energizing effect to that without self-energizing effect, knowing that physical parameters—friction coefficient and clutch dimension—are consistent.

Based on (1), the relationship between the clutch torque and actuation torque at steady state can be expressed as follows:

$$T_a = 2r_p F_n \tan \alpha - T_c. \quad (11)$$

Substitution of (11) into (9) then gives

$$G_a = \frac{T_c}{2r_p F_n \tan \alpha - T_c}. \quad (12)$$

Applying (8) to (12) and simplifying the result by assuming that $r_p \approx R_c$ leads to the following expression of the actuation

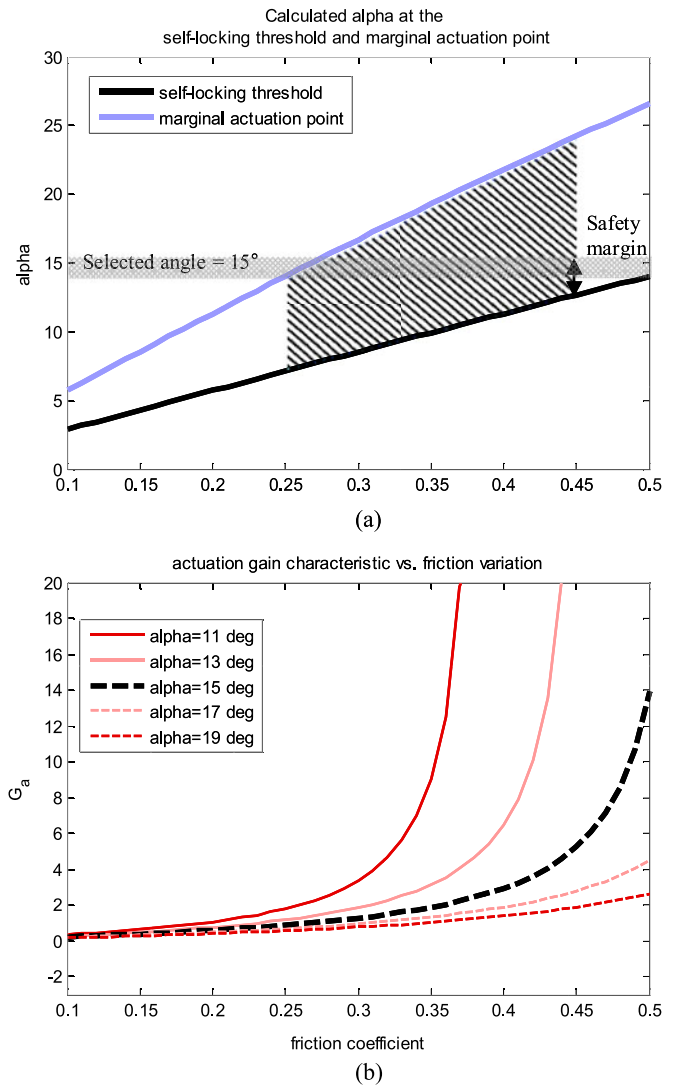


Fig. 6. Self-energizing clutch actuator characteristics. (a) Plot of calculated alpha at the self-locking threshold and marginal actuation point against friction coefficient. (b) Plot of actuation gain against friction coefficient.

gain:

$$G_a = \frac{\mu}{2 \tan \alpha - \mu}. \quad (13)$$

Since the system tends to rapidly become self-locking (infinite G_a) near the point where $\mu = 2 \tan \alpha$, this point—henceforth, referred to as the self-locking threshold—must be avoided for effective control of the clutch engagement. On the other hand, strong engagement becomes difficult with insufficient actuation gain. So the point where $G_a = 1$ is henceforth referred to as the marginal actuation point. It is preferred that the system maintains greater actuation gain than that at the marginal actuation point.

Along the self-locking threshold, the rack inclination angle α is calculated and plotted against varying friction coefficient μ , and it is shown in black curve in Fig. 6(a). Also, along the marginal actuation point, α is plotted on the same axis in thick light blue. The operation point must stay above the thick black curve to avoid self-locking and preferably stays

below the thick light-blue curve to secure sufficient engagement force. Considering that the clutch friction coefficient typically stays within the range of 0.25–0.45, depending on the surface temperature and the slip speed, the shaded region in Fig. 6(a) represents the appropriate operation point.

The friction coefficient μ may vary, but the inclination angle α must be selected and fixed. Hence, for the operation point to stay inside the shaded region even with μ varying from 0.25 to 0.45, α can only be selected in the narrow range around 13°–15°. To provide some safety margin from the self-locking point as indicated in Fig. 6(a), the actuator is designed with $\alpha = 15^\circ$. The plots of actuation gain G_a against μ for different α are also plotted in Fig. 6(b). It can be assured that for the case of $\alpha = 15^\circ$, rapid increase in G_a does not take place within the plausible μ range. It must be noted that this α is selected for the specific clutch-facing material which has its friction coefficient between 0.25 and 0.45. In order to cope effectively with other types of clutch-facing materials that involve a different range of friction coefficient, the appropriate value of α must be recalculated.

Now, the theoretical value for the torque amplification gain G_t is calculated using the selected α . For the case without the self-energizing effect, simply the clutch torque term can be eliminated from (1) to describe the actuator model, since the nonenergizing case is characterized by the state in which the clutch torque has no effect on the actuation dynamics. Hence, at steady state, the following expression for the actuation torque can be achieved:

$$T_a = 2r_p F_n \tan \alpha. \quad (14)$$

When (14) is equated with (11), the expression of the actuation torque in the presence of self-energizing effect, the following holds, given that the actuation torque is consistent

$$\begin{aligned} F_{n,\text{self-energizing}}(2r_p \tan \alpha - \mu R_c) = \\ 2F_{n,\text{self-energizing}} r_p \tan \alpha. \end{aligned} \quad (15)$$

From (15), based on the definition of the torque amplification gain in (10), it can be obtained as shown next

$$G_t = \frac{2r_p \tan \alpha}{2r_p \tan \alpha - \mu R_c} \approx 2.88. \quad (16)$$

Here, $\alpha = 15^\circ$ and $\mu = 0.35$ are used to calculate the theoretical torque amplification gain. The result indicates that the designed system is capable of transmitting up to 2.88 times the maximum torque achieved by the system without self-energizing effect.

C. Driveline Model for Test Bench

A six-DOF model is established to describe the driveline, and the schematic illustration of this model is shown in Fig. 7.

This driveline model can be mathematically represented by using the following series of torque balance equations:

$$J_e \dot{\omega}_e = T_e - T_d \quad (17)$$

$$J_d \dot{\omega}_d = T_d - T_{c1} - T_{c2} \quad (18)$$

$$J_{e1} \dot{\omega}_{c1} = T_{c1} - \frac{T_{t1}}{i_{t1}} \quad (19)$$

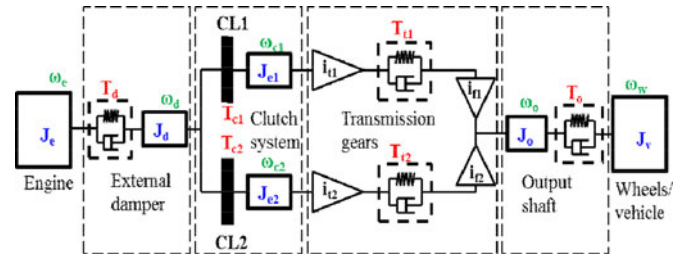


Fig. 7. Model of the driveline with DCT system (J : inertia, T : torque, ω : angular velocity).

$$J_{e2} \dot{\omega}_{c2} = T_{c2} - \frac{T_{t2}}{i_{t2}} \quad (20)$$

$$J_o \dot{\omega}_o = i_{f1} T_{t1} + i_{f2} T_{t2} - T_o \quad (21)$$

$$J_v \dot{\omega}_w = T_o - T_v. \quad (22)$$

Here, J_{e1} and J_{e2} refer to the effective transmission inertia of the components attached on the input shaft, and those on input shaft 2, respectively. For each dynamics, the related torque is modeled in terms of the torsional compliance [30]–[32] as follows:

$$T_e = f(\alpha_{th}, \omega_e) \quad (23)$$

$$T_d = k_d (\theta_e - \theta_d) + b_d (\omega_e - \omega_d) \quad (24)$$

$$T_{c1} = \mu R_{c1} F_{n1} \text{sgn}(\omega_d - \omega_{c1}) \quad (25)$$

$$T_{c2} = \mu R_{c2} F_{n2} \text{sgn}(\omega_d - \omega_{c2}) \quad (26)$$

$$T_{t1} = k_{t1} \left(\frac{\theta_{c1}}{i_{t1}} - i_{f1} \theta_o \right) + b_{t1} \left(\frac{\omega_{c1}}{i_{t1}} - i_{f1} \omega_o \right) \quad (27)$$

$$T_{t2} = k_{t2} \left(\frac{\theta_{c2}}{i_{t2}} - i_{f2} \theta_o \right) + b_{t2} \left(\frac{\omega_{c2}}{i_{t2}} - i_{f2} \omega_o \right) \quad (28)$$

$$T_o = k_o (\theta_o - \theta_w) + b_o (\omega_o - \omega_w) \quad (29)$$

$$\begin{aligned} T_v = r_w \left(\underbrace{m_v g \sin(\theta_{\text{road}})}_{\text{road gradient}} + \underbrace{K_{rr} m_v g \cos(\theta_{\text{road}})}_{\text{rolling resistance}} \right. \\ \left. + \underbrace{\frac{1}{2} \rho v_x^2 C_d A}_{\text{aerodynamic drag}} \right). \end{aligned} \quad (30)$$

Here, θ_{road} , K_{rr} , m_v , ρ , v_x , C_d , and A indicate the road gradient angle, the tire rolling resistance, the vehicle mass, the air density, the vehicle velocity, the aerodynamic drag coefficient, and the vehicle frontal area, respectively. These are the variables that must be included for modeling the driveline of an actual vehicle. However, those that are not applicable to the test bench driveline are excluded and only the frictional loss acting the inertia disk is modeled to express (30).

The key feature of the developed model is that the actuator model is linked to the driveline model to reflect the self-energizing effect. In other words, the clutch torques modeled in (25) and (26) are used in the motor dynamics shown in (3) as feedback.

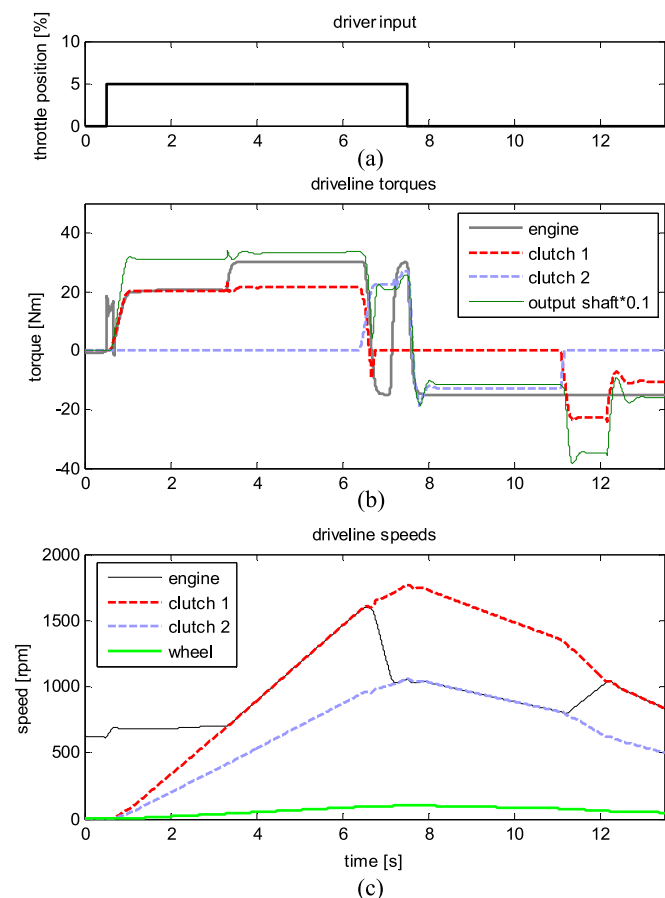


Fig. 8. Simulation scenario 1. (a) Throttle input. (b) Driveline torques. (c) Driveline speeds.

IV. SIMULATION AND EXPERIMENTS

A. Simulation

Using simulation, actuator energy consumption with self-energizing effect and that without self-energizing effect are compared. For accurate comparison, identical PID controllers are used for both cases. Also, since the self-energizing mechanism may lead to de-energizing effect as well when the direction of clutch torque and actuation torque are opposite, simulation scenario should cover all of the low-load/high-load, upshift/downshift, and accelerating/braking conditions for fair comparison. Here, the de-energizing effect refers to the state in which the torque transmitted through the clutch adversely affects the actuation effort. It must be noted that, the states shown in the following simulation scenarios are achieved by conducting the simulation for the self-energizing case. For the nonenergizing case, the clutch torque term is eliminated from the actuator motor's dynamic model in (3).

The first simulation scenario shown in Fig. 8 includes low-load condition in which driver's input remains at 5% throttle which is followed by deceleration due to engine brake. Like in the production cars, the engine torque is deliberately reduced during the upshift to match the speed in this scenario. Such scenario is to check the reduced actuation energy consumption by self-energizing effect, and the increased actuation energy consumption by de-energizing effect. The actuation energy is

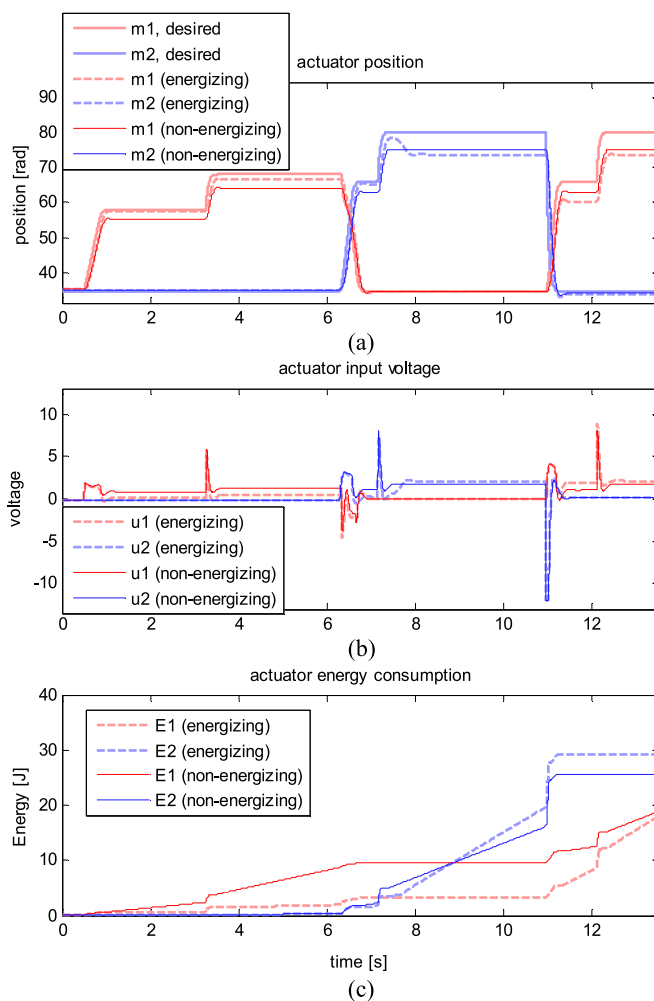


Fig. 9. Simulation result 1. (a) Desired and measured actuator position. (b) Actuator input. (c) Cumulative actuator energy consumption.

calculated by integrating the input power over time, and the input power is obtained from the product of the control input voltage and motor current calculated based on (5).

Observation of the simulation results for actuator energy consumption displayed in Fig. 9 indicates that actuator 1 uses more energy without self-energizing effect than that with self-energizing effect. This is because the clutch actuator must exert torque in the engaging direction to launch the vehicle, and the transmitted positive torque facilitates the actuation in the direction of engagement as modeled in (1). This phenomenon continues even when the clutch completely engaged.

During the upshift around 6–7 s, actuator 2 uses more energy without self-energizing effect as well. This is because, again, the second clutch is being engaged as positive torque is transmitted through it.

Notice that the opposite happens in case of the off-going clutch 1. Fig. 8(b) indicates that positive torque is still being transmitted by clutch 1 when actuator 1 attempts to disengage the clutch. Here, the directions of actuation torque and clutch transmitted torque are opposite, and the actuator uses more energy in the presence of self-energizing effect than that without it.

Energy consumption in actuator 2 with self-energizing effect exceeds that without it around 9 s. This is because the engine

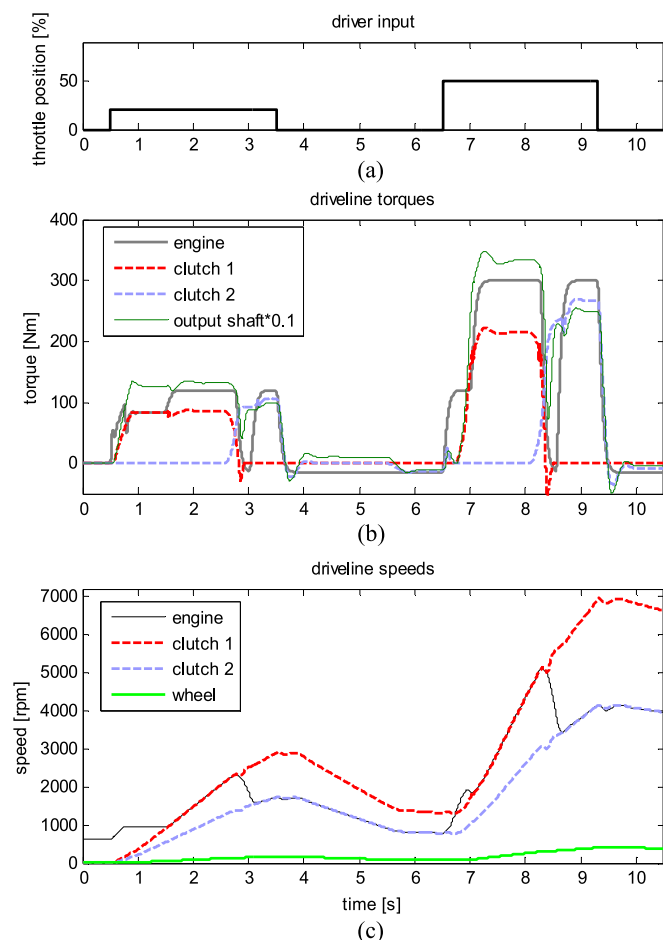


Fig. 10. Simulation scenario 2. (a) Throttle input. (b) Driveline torques. (c) Driveline speeds.

brake causes negative torque to be transferred through clutch 2 while actuator 2 applies positive actuation torque on the pressure plate. Similar principle applies to actuator 1 during the downshift around 11 s as well.

It is now confirmed that the suggested actuator consumes less energy during actuation process when the directions of actuation torque and clutch transmitted torque are the same, and more energy when the directions of actuation torque and clutch transmitted torque are opposite. One may then argue that cumulative sum of the consumed energy over repeated cycles of upshifts and downshifts using the suggested actuator system would not be much less than that without the suggested self-energizing mechanism. However, it must be clear that the amount of energy saving becomes more distinguished in cases of high-load conditions. After all, the magnitude of the average positive torque transferred through the clutches is distinctly greater than the magnitude of the average negative torque transferred through the clutches, so the overall actuation efficiency can be improved.

To validate such claim, the next simulation scenario shown in Fig. 10 includes launch and upshift performed with 20% throttle input, braking, followed by a downshift and upshift with 50% throttle input and engine braking.

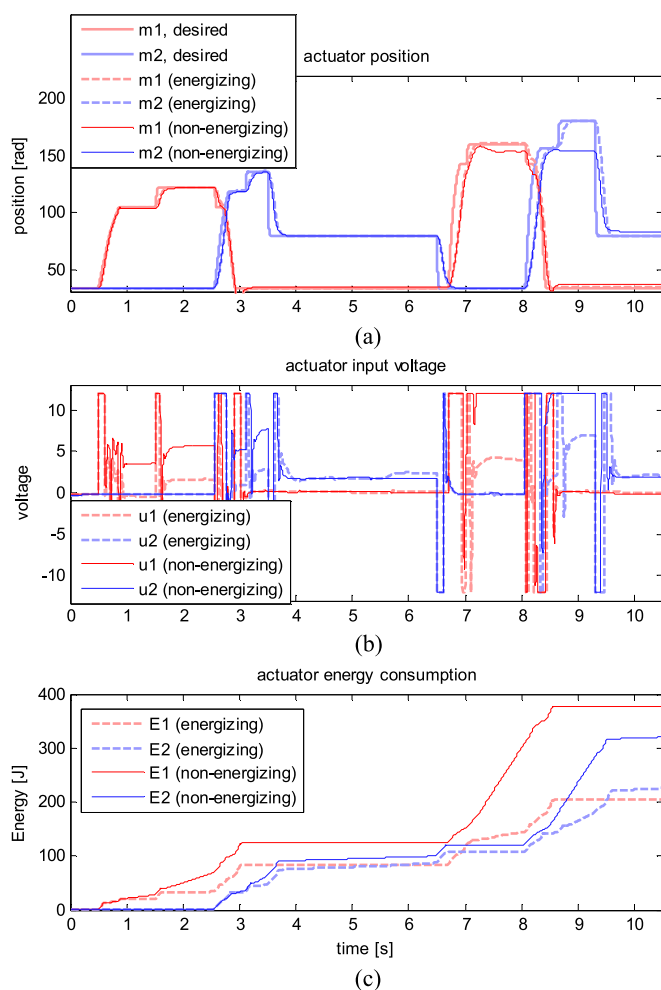


Fig. 11. Simulation result 2. (a) Desired and measured actuator position. (b) Actuator input. (c) Cumulative actuator energy consumption.

As Fig. 11(c) shows, significant amount of energy is saved by using the self-energizing clutch actuator in both actuator 1 and 2 for the case of launch and the first upshift around 3 s. As expected, slightly more energy is consumed by the self-energizing actuator 1 during the upshift because of the aforementioned reason explained for the first scenario. Overall, the energy consumption difference which happened during the unfavorable condition for the self-energizing system is unnoticeable, since the amount of energy saving achieved during the favorable conditions overwhelms it.

The amount of energy saved becomes even greater when 50% throttle is applied from around 6.5 s. During the power-on downshift unlike the downshift which took place in the first simulation scenario, the inertia phase comes before the torque phase in order to prevent clutch tie-up. This implies that the clutch torque is constantly in the same direction as the actuation torque, and the self-energizing effect becomes extremely useful.

Observing Fig. 11 during this time range tells that both non-energizing actuators 1 and 2 fail to follow the desired actuator motor trajectory, even with control input saturated at maximum. On the other hand, however, both self-energizing actuators 1 and 2 successfully follow the desired actuator motor trajectory [see Fig. 11(a)], and the control input is not saturated [see Fig. 11(b)].

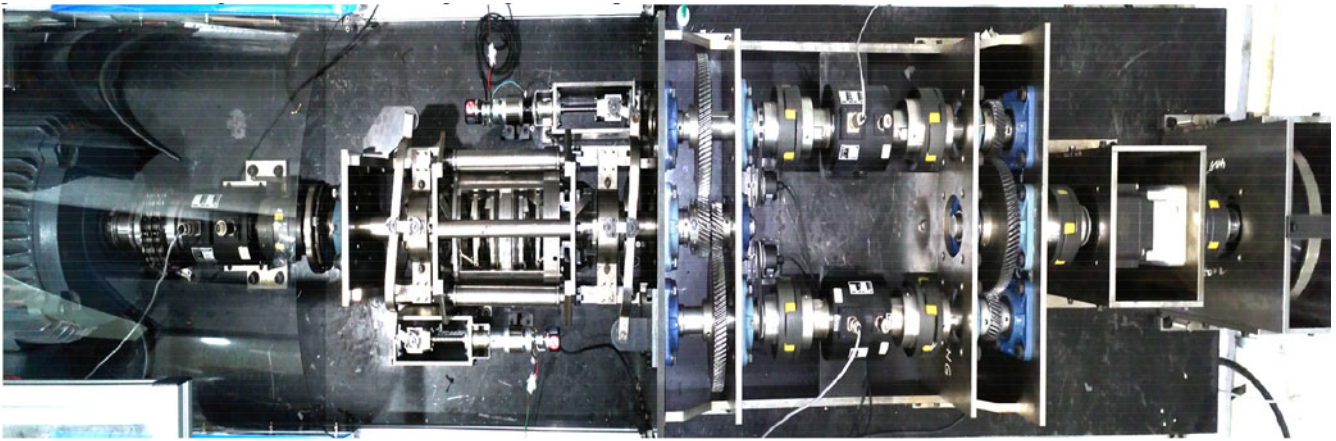


Fig. 12. Driveline test bench.

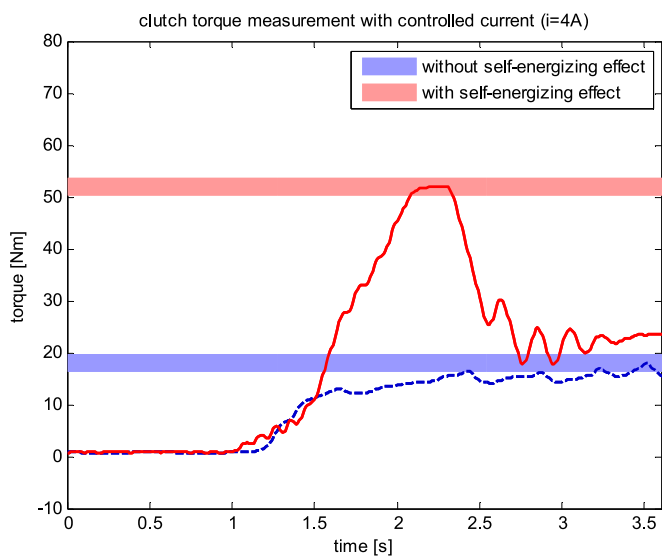


Fig. 13. Result of validation experiment for torque amplification gain.

B. Test Bench Experiment

In addition to the simulation, experiments are conducted as well to validate the claims formulated by designing and modeling the self-energizing clutch actuator. Fig. 12 shows the photograph of the driveline test bench constructed for experiments. MicroAutobox dSPACE 1401 is used to run the control software and to process the signals from the sensors. DC motors with the rated output of 41.3 W are chosen for actuator motors. Considering that conventional dry DCT actuators have the rated output of up to 300 W, significant reduction in the motor size requirement is achieved.

The result of the experiment which validates the torque amplification gain claimed in (16) is shown in Fig. 13. As expected, the experimentally obtained ratio of maximum torque obtained by using the self-energizing actuator to that obtained by using the nonenergizing actuator is equivalent to the ratio calculated from the actuator model.

Here, in order to intentionally eliminate the self-energizing effect, controlled current of 4 A is first applied to the actuator

without turning on the ac motor (engine). When the actuator reaches its maximum position, the motor is anchored at this point. Then ac motor starts running so that torque can finally begin to be transmitted through the clutch whose engagement force is fixed at the point reached in the absence of the self-energizing effect. The transmitted clutch torque is recorded and plotted in dotted blue line in Fig. 13.

On the other hand, in case of conducting the experiment in presence of the self-energizing effect, the same degree of controlled current is applied to the actuator motor when the ac motor is already running. The torque transmitted through the clutch is then recorded and plotted in solid red line in Fig. 13. The transmitted torque is reduced soon after reaching the maximum torque, because the clutch slip rapidly converges to zero due to high torque.

In addition to the torque amplification gain verification, actuator energy consumption is checked by conducting launch and gear shift scenario displayed in Fig. 14. It must be noted that, the driveline states shown in Fig. 14 are achieved by conducting the experiment for the self-energizing case. For the nonenergizing case, actuators were made to follow the desired trajectories without running the ac motor (engine) so that the self-energizing effect did not take place.

Similar to the case of simulation, the experiment includes low-load condition in which driver's input remains at 10% throttle which is followed by deceleration due to engine brake. Again, the actuation energy is calculated by integrating the input power over time, and the input power is obtained from the product of the control input voltage. The motor current is calculated based on (5) by using the known motor parameters and motor speed measurements.

Just as expected, the energy consumption plotted in Fig. 15(c) shows that the self-energizing clutch actuator had advantage during clutch 1 engagement for launch, and clutch 2 engagement for upshift. Also, as discussed in Section IV-A, the nonenergizing clutch actuator had advantage during clutch 1 disengagement for upshift, and clutch 2 engagement for downshift.

However, the amount of energy saved by the self-energizing clutch actuator increases abruptly as the load on the actuator increases. Indeed, vast difference in energy consumption can be

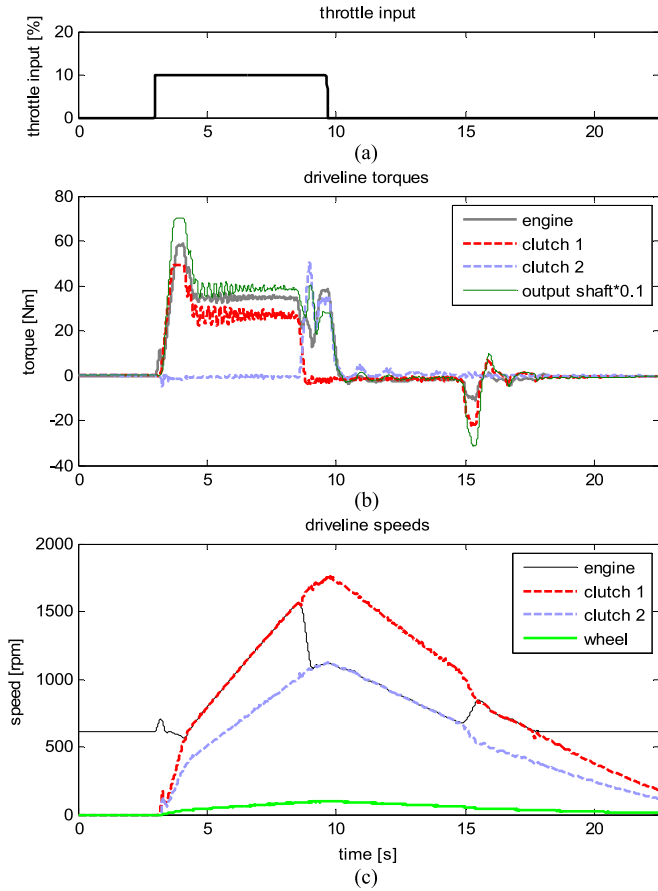


Fig. 14. Experiment scenario. (a) Throttle input. (b) Driveline torques. (c) Driveline speeds.

observed in Fig. 15(c) for the case of clutch 2 engagement after upshift, and the total amount of energy consumption is greater in case of the nonenergizing clutch actuator.

V. CONCLUSION

This study has proposed a novel clutch actuator for dry-type DCT using self-energizing mechanism. Making use of the pinion and inclined rack gears, the actuator is designed so that the positive torque transmitted through the clutch adds to the actuation torque acting on the pressure plate. Summarizing the paper, noteworthy contributions of the proposed work are the following: the novel design of the self-energizing clutch mechanism for DCT, experimental validation of the torque amplification gain, and thorough examination of the proposed actuator's application potential on DCT by analyzing the advantage of reduced actuator energy consumption during launch and gear shifts conducted by DCT. The results of the simulations and experiments have revealed that while the self-energizing clutch actuator consumes slightly more energy than the nonenergizing actuator when the directions of the clutch torque and actuation torque are opposite, the self-energizing clutch actuator saves significant amount of energy compared to the nonenergizing actuator when the directions of the clutch torque and actuation torque are the

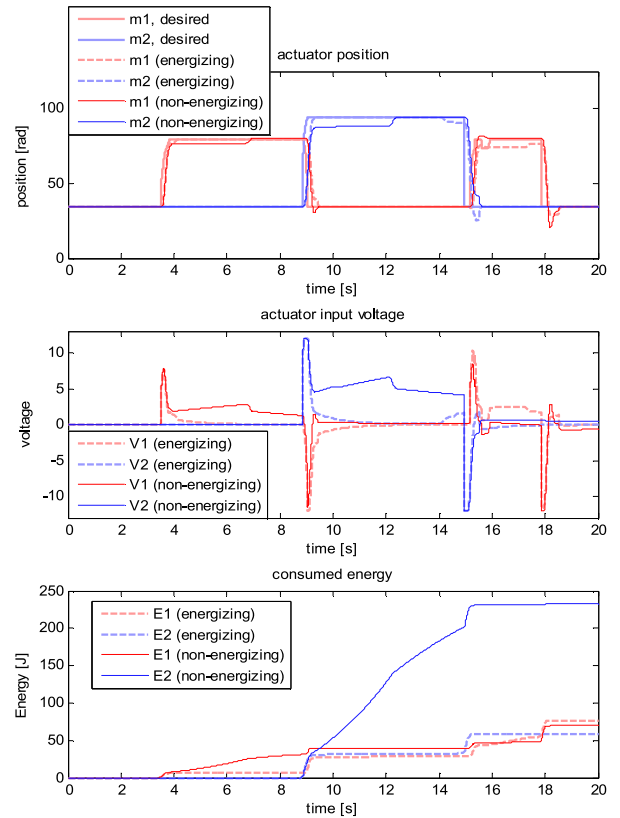


Fig. 15. Experiment result. (a) Desired and measured actuator position. (b) Actuator input. (c) Cumulative actuator energy consumption.

same. Also, it is experimentally verified that the advantage of the self-energizing actuator over the nonenergizing one regarding its energy consumption increases as the clutch-transferred torque increases. Hence, the overall actuator efficiency is higher in case of the self-energizing clutch actuator, since magnitude of the positive driving torque is much greater than that of the negative torque caused by the engine brake. The application of the proposed actuator shall require effective control tactics to cope with the increased system sensitivity for accurate tracking control of the desired torque command.

APPENDIX SYSTEM PARAMETERS

Parameter	Value	Parameter	Value
L_m	0.4 mH	J_o	0.04 kg-m ²
k_e	0.016 V-s/rad	J_v	134.6 kg-m ²
k_t	0.016 N-m/A	i_{t1}	3
R_m	0.9 Ω	i_{t2}	2.4
J_a^*	4×10^{-5} kg-m ²	i_{f1}	6
r_p	0.095 m	i_{f2}	4.8
R_c	0.095 m	k_{t1}	1.5×10^4 N-m/rad
N_{ae}	944	b_{t1}	50 N-m-s/rad
J_e	0.745 kg-m ²	k_{t2}	1.5×10^4 N-m/rad
J_d	0.0165 kg-m ²	b_{t2}	50 N-m-s/rad
J_{e1}	0.1 kg-m ²	k_o	1.0×10^4 N-m/rad
J_{e2}	0.1 kg-m ²	b_o	700 N-m-s/rad

REFERENCES

- [1] L. Gaertner and M. Ebenhoch, "The ZF automatic transmission 9HP48 transmission system, design and mechanical parts," *SAE Int. J. Passenger Cars Mech. Syst.*, vol. 6, no. 2, pp. 908–917, 2013.
- [2] P. Setlur, J. R. Wagner, D. M. Dawson, and B. Samuels, "Nonlinear control of a continuously variable transmission (CVT)," *IEEE Trans. Control Syst. Technol.*, vol. 11, no. 1, pp. 101–108, Jan. 2003.
- [3] J. Ji, M. J. Jang, O. E. Kwon, M. J. Chai, and H. S. Kim, "Power transmission dynamics in micro and macro slip regions for a metal v-belt continuously variable transmission under external vibrations," *Int. J. Autom. Technol.*, vol. 15, no. 7, pp. 1119–1128, Dec. 2014.
- [4] P. Spanoudakis and N. C. Tsourveloudis, "Prototype variable transmission system for electric vehicles: Energy consumption issues," *Int. J. Autom. Technol.*, vol. 16, no. 3, pp. 525–537, Mar. 2015.
- [5] L. Glielmo, L. Iannelli, V. Vacca, and F. Vasca, "Gearshift control for automated manual transmissions," *IEEE/ASME Trans. Mechatronics*, vol. 11, no. 1, pp. 17–26, Feb. 2006.
- [6] M. Pisaturo, M. Cirrincione, and A. Senatore, "Multiple constrained MPC design for automotive dry clutch engagement," *IEEE/ASME Trans. Mechatronics*, vol. 20, no. 1, pp. 469–480, Feb. 2015.
- [7] K. Zhao, Y. Liu, X. Huang, R. Yang, and J. Wei, "Uninterrupted shift transmission and its shift characteristics," *IEEE/ASME Trans. Mechatronics*, vol. 19, no. 1, pp. 374–383, Feb. 2014.
- [8] K. van Berkel, F. Veldpaus, T. Hofman, B. Vroemen, and M. Steinbuch, "Fast and smooth clutch engagement control for a mechanical hybrid powertrain," *IEEE Trans. Control Syst. Technol.*, vol. 22, no. 4, pp. 1241–1254, Jul. 2014.
- [9] H. Zhang, Z. Zhong, and X. Chen, "Systematic synthesis method and prototyping of fixed-axle vehicular electrified mechanical transmission," *Int. J. Autom. Technol.*, vol. 16, no. 4, pp. 697–705, Aug. 2015.
- [10] S. J. Kim, C. Song, K. -S. Kim, and Y. -S. Yoon, "Analysis of the shifting behavior of a novel clutchless geared smart transmission," *Int. J. Autom. Technol.*, vol. 15, no. 1, pp. 125–134, Feb. 2014.
- [11] J. J. Oh and S. B. Choi, "Real-time estimation of transmitted torque on each clutch for ground vehicles with dual clutch transmission," *IEEE/ASME Trans. Mechatronics*, vol. 20, no. 1, pp. 24–36, Feb. 2015.
- [12] N. Kim, H. Lohse-Busch, and A. Rousseau, "Development of a model of the dual clutch transmission in autonomie and validation with dynamometer test data," *Int. J. Autom. Technol.*, vol. 15, no. 2, pp. 263–271, Mar. 2014.
- [13] M. Kulkarni, T. Shim, and Y. Zhang, "Shift dynamics and control of dual-clutch transmissions," *Mech. Mach. Theory*, vol. 42, no. 2, pp. 168–182, 2007.
- [14] P. D. Walker, N. Zhang, and R. Tamba, "Control of gear shifts in dual clutch transmission powertrains," *Mech. Syst. Signal Process.*, vol. 25, no. 6, pp. 1923–1936, 2011.
- [15] M. Goetz, M. C. Levesley, and D. A. Crolla, "Dynamics and control of gearshifts on twin-clutch transmissions," *Proc. Inst. Mech. Eng. D: J. Autom. Eng.*, vol. 219, no. 8, pp. 951–963, 2005.
- [16] X. Song, C. S. Wu, and Z. Sun, "Design, modeling, and control of a novel automotive transmission clutch actuation system," *IEEE/ASME Trans. Mechatronics*, vol. 17, no. 3, pp. 582–587, Jun. 2012.
- [17] Z. G. Zhao, J. L. Jiang, Z. P. Yu, T. Zhang, "Starting sliding mode variable structure that coordinates the control and real-time optimization of dry dual clutch transmissions," *Int. J. Automotive Technol.*, vol. 14, no. 6, pp. 875–888, Dec. 2013.
- [18] M. X. Wu, J. W. Zhang, T. L. Lu, and C. S. Ni, "Research on optimal control for dry dual-clutch engagement during launch," *Proc. Inst. Mech. Eng. D: J. Autom. Eng.*, vol. 224, no. 6, pp. 749–763, 2010.
- [19] X. Song and Z. Sun, "Pressure-based clutch control for automotive transmissions using a sliding-mode controller," *IEEE/ASME Trans. Mechatronics*, vol. 17, no. 3, pp. 534–546, Jun. 2012.
- [20] A. Myklebust and L. Eriksson, "Modeling, observability, and estimation of thermal effects and aging on transmitted torque in a heavy duty truck with a dry clutch," *IEEE/ASME Trans. Mechatronics*, vol. 20, no. 1, pp. 61–72, Feb. 2015.
- [21] T. Welge-Luessen and C. Glocker, "Modelling and application of the self-locking phenomenon in the context of a non-discrete impact clutch," *PAMM*, vol. 5, no. 1, pp. 221–222, Dec. 2005.
- [22] G. J. Organek and D. M. Preston, "Driveline clutch with unidirectional apply ball ramp," U.S. Patent 5 810 141, Sep. 22, 1998.
- [23] Y. Jian, L. Chen, F. Liu, and C. Yin, "Experimental study on improvement in the shift quality for an automatic transmission using a motor-driven wedge clutch," *Proc. Inst. Mech. Eng. D: J. Autom. Eng.*, vol. 228, no. 6, pp. 663–673, 2014.
- [24] J. Kim and S. B. Choi, "Design and modeling of a clutch actuator system with self-energizing mechanism," *IEEE/ASME Trans. Mechatronics*, vol. 16, no. 5, pp. 953–966, Oct. 2011.
- [25] S. B. Choi and J. Kim, "Disk friction clutch apparatus using self-energizing effect," U.S. Patent 8 348 038, Jan. 8, 2013.
- [26] S. B. Choi and J. Oh, "Self-energizing clutch by using direct-pinion-controlling method, and dual clutch apparatus using the clutch," Korea Patent 1 013 962 590 000, May 12, 2014.
- [27] S. Sfarni, E. Bellenger, J. Fortin, and M. Malley, "Numerical and experimental study of automotive riveted clutch discs with contact pressure analysis for the prediction of facing wear," *Finite Elements Anal. Design*, vol. 47, no. 2, pp. 129–141, 2011.
- [28] N. Cappetti, M. Pisaturo, and A. Senatore, "Modelling the cushion spring characteristic to enhance the automated dry-clutch performance: The temperature effect," *Proc. Inst. Mech. Eng. D: J. Autom. Eng.*, vol. 226, no. 11, pp. 1472–1482, Nov. 2012.
- [29] C. D. Wit, H. Olsson, K. Astrom, and P. Lischinsky, "A new model for control of systems with friction," *IEEE Trans. Autom. Control*, vol. 40, no. 3, pp. 419–425, Mar. 1995.
- [30] Y. Liu, D. Qin, H. Jiang, and Y. Zhang, "A systematic model for dynamics and control of dual clutch transmissions," *J. Mech. Design*, vol. 131, p. 061012, 2009.
- [31] C. Ni, T. Lu, and J. Zhang, "Gearshift control for dry dual-clutch transmissions," *WSEAS Trans. Syst.*, vol. 8, no. 11, pp. 1177–1186, 2009.
- [32] P. D. Walker and N. Zhang, "Modelling of dual clutch transmission equipped powertrains for shift transient simulations," *Mech. Mach. Theory*, vol. 60, pp. 47–59, 2013.



Jiwon J. Oh received the Bachelor's and M.S. degrees in mechanical engineering from the Korea Advanced Institute of Science and Technology (KAIST), Daejeon, Korea, where he is currently working toward the Ph.D. degree in mechanical engineering.

His current research interests include vehicle driveline state estimation and dual-clutch transmission control.



Jinsung Kim (S'10–M'13) received the Ph.D. degree in mechanical engineering from the Korea Advanced Institute of Science and Technology (KAIST), Daejeon, Korea, in 2013.

He is currently a Senior Research Engineer with the Research and Development Center, Hyundai Motor Company, Hwasung, Korea, where he is currently involved in designing clutch control algorithms of a seven-speed dual-clutch transmissions for production vehicles. His current research interests include automotive systems, nonlinear control, and integrated design and control of complex mechanical systems.



Seibum B. Choi (M'09) received the B.S. degree in mechanical engineering from Seoul National University, Seoul, Korea, the M.S. degree in mechanical engineering from the Korea Advanced Institute of Science and Technology (KAIST), Daejeon, Korea, and the Ph.D. degree in controls from the University of California, Berkeley, in 1993.

From 1993 to 1997, he was involved in the development of automated vehicle control systems at the Institute of Transportation Studies, University of California, Berkeley. During 2006, he was with TRW, Warren, MI, USA, where he was involved in the development of advanced vehicle control systems. Since 2006, he has been with the faculty of the Mechanical Engineering Department, KAIST. His current research interests include fuel-saving technology, vehicle dynamics and control, and active safety systems.